ADVANCED MATERIALS TECHNOLOGIES
www.advmattechnol.de

Wearable Humidity Sensor for Continuous Sweat Rate Monitoring

*Ashwin Aggarwal, Manik Dautta, Luis Fernando Ayala-Cardona, Aalaya Wudaru, and Ali Javey**

The rapid advancements in wearable technologies are allowing for personal and tailored monitoring systems for core bodily metrics. Modern smartwatches accurately and frequently stream physical signals such as heart rate and respiratory rate. However, smartwatches have yet to track a multitude of physiological parameters, including sweat rate. This work presents a new wearable device that tracks sweat rate, the body's most important thermoregulatory function. The device is tape-free and utilizes an off-the-shelf humidity sensor, with the potential to be integrated with existing smartwatch bands. It features a 3D-printed chamber with a humidity sensor and microheater, and it interfaces the skin with a malleable and concave sweat collector. Through various experiments and trials, the authors seek to understand the relationship between sweat-induced humidity within the chamber and the amount of sweat secreted when worn. Compared to existing sweat rate sensing devices, this hygrometer-based device can be worn for extensive periods of time without overfilling. The device's reusability and compactness make it a good candidate for use alongside modern, microfluidic-based sweat rate devices.

1. Introduction

Wearable healthcare technologies have become increasingly prevalent in recent years, allowing individuals to monitor their physiological state without the need for bulky equipment or medical professionals. For the most part, wearable devices have the ability to monitor physiological signals such as heart rate, body temperature, blood oxygen, and activity.[1–5] However, to gain more in-depth health information, researchers have shifted their focus to novel signals, one of which is sweat. Sweat is rich in analytes such as ions and metabolites. As a result, sweat has been subject to extensive correlative studies, which has sparked interest in wearable, reliable, and continuous modes for sensing sweat composition and secretion rate. Recent promising correlations between sweat composition and blood glucose levels, levodopa profiles, and dehydration levels have demonstrated the immense potential of personalized wearable sweat sensors.[6–11] In addition to sweat composition, the continuous tracking of regional sweat rate can provide insights into underlying physical conditions such as hyperhidrosis or hypohidrosis.[12–15] In the area of sports medicine, sweat rate helps assess dehydration levels in athletes so they can rehydrate accordingly.[16–18] In addition, standalone sweat rate profiles can also indicate signs of autonomic dysfunction, a common symptom among ischemic stroke patients.[19,20] When both sweat composition and sweat rate are measured continuously in tandem, the full potential of these preventative and restorative measures can be realized.

Currently, gravimetric testing methods such as the quantitative pilocarpine iontophoresis test or the quantitative sudomotor axon reflex test are most commonly used for measuring total sweat loss.[21] These methods first induce sweating in sweat gland–dense regions with electrical or chemical stimuli and then use a sweat collector such as a Macroduct to collect the total amount of sweat secreted. While they are clinically validated, these methods have to be performed off-body and in specialized settings with the intervention of trained experts, which delays the availability of the results to patients. Wearable sweat rate devices, on the other hand, can provide sweat loss measurements in real-time and have the advantage of being portable and user-friendly. Currently, there are multiple types of wearable sweat rate sensors available, including microfluidic-based and hygrometer-based devices.

A. Aggarwal, M. Dautta, A. Javey
Department of Electrical Engineering and Computer Sciences
University of California
Berkeley, CA 94720, USA
E-mail: ajavey@berkeley.edu

A. Aggarwal, M. Dautta, L. F. Ayala-Cardona, A. Javey
Berkeley Sensor and Actuator Center
University of California
Berkeley, CA 94720, USA

L. F. Ayala-Cardona, A. Wudaru
Department of Bioengineering
University of California
Berkeley, CA 94720, USA

A. Javey
Materials Sciences Division
Lawrence Berkeley National Laboratory
Berkeley, CA 94720, USA

The ORCID identification number(s) for the author(s) of this article can be found under https://doi.org/10.1002/admt.202300385

DOI: 10.1002/admt.202300385

Microfluidic-based sensors usually come in two main form factors: an adhesive patch or a tape-free configuration.[22] Patch sensors are made of flexible layers, affixed to the skin using an adhesive backing.[23–30] These types of sensors are often reliable, easy to use, and have been reported to operate for up to 20 h at once.[24,28] Commercially available wearable sweat rate sensor today is a kind of colorimetric, microfluidic, and patched-based sensor.[29] While this sensor allows for insights into an individual's dehydration levels and fluid loss, it relies on the user to manually take a photo of the device to calculate their overall sweat rate at the end of an exercise period. In addition, these patch-based sensors are usually single-use and have a maximum fluid capacity. Nevertheless, device integrations into microfluidic channels address the issue of low temporal resolution and maximum volume capacity in patch-based sensors. For example, researchers have developed a calorimetric microfluidic flow sensor that integrates with the inlet of a microfluidic system, resolving the issue of channel saturation.[31] With a wireless chip, this device transmits continuous data to a smartphone, providing real-time sweat rate measurements. Researchers have also developed a digital droplet flow rate sensor that integrates with the outlet of a microfluidic channel, which allows a volumetric resolution in the nanoliter scale.[32] This device demonstrated a great dynamic range of measured flow rates and the ability to run for long periods of time since measurements are independent of the channel volume capacity. However, these microfluidic-based devices and integration techniques may suffer from the presence of air bubbles and sodium buildup, which can affect sweat rate calculations. Moreover, some users may find these adhesive-based patches to be uncomfortable or irritating, especially if worn for an extended period of time. Tape-free sensors, on the other hand, are designed to be worn without any adhesive backing. Instead, they use a malleable sweat collector to secure the sensor to the skin. These types of sensors can often be more comfortable to wear and durable than adhesive-based patch sensors. In our previous work, we developed a tape-free device that uses impedimetric measurements to calculate a user's continuous sweat rate during exercise periods.[22] While larger-scale studies have yet to be conducted with this form-factor, these device designs present promising opportunities for integration with existing smartwatch bands

Furthermore, current hygrometer-based devices aim to measure sweat rate by analyzing the relative humidity at the skin's surface when a user sweats. These types of sensors come in two different configurations: open-chamber and closed-chamber. Open-chamber hygrometer-based sensors that use two humidity sensors to analyze sweat rate have shown promising results.[33] However, open-chamber devices suffer from their dependence on stable ambient temperatures and humidities, which severely affects their sweat rate calculation abilities. On the other hand, closed-chamber sensors operate well in variable ambient conditions, but they suffer from a lack of ventilation, which limits these devices' ability to monitor sweat-induced humidity levels when worn for exercise or long periods of time.

In this work, we present a wearable hygrometer-based sweat rate sensor that uses an off-the-shelf humidity sensor enclosed by a chamber with ventilation holes. This device is adhesive-free and can be integrated with existing wearable platforms such as smartwatches or fitness trackers. Similar to our previous work, this device consists of a 3D-printed body with a sweat collector, but now it features a chamber that houses a humidity sensor and a microheater. This tape-free hygrometer-based sweat rate sensor provides a potential alternative to the adhesive and microfluidic-based platforms, as it offers continuous access to sweat rate monitoring and reusability, which could lead to its widespread use as a consumer product.

2. Results and Discussion

2.1. Device Structure

Our humidity-based sweat collection device, shown in **Figure 1**a, is designed to capture sweat and measure the sweat-induced humidity levels. The device is composed of two primary sections, the sweat collection well and the humidity chamber (Figure 1b). The sweat collection well, which enables sweat from the skin to enter the device, is 3D-printed with a rubber-like and flexible material that creates a watertight and comfortable seal with the skin's surface when worn. The elliptically shaped and curvilinear architecture allows for sweat to accumulate before entering the inlet, ensuring the collection of sweat from a multitude of sweat glands. As the user begins to sweat, the sweat's secretion pressure pushes the liquid through the collector's inlet and into the humidity chamber. This hard-surfaced and hollow container resides on top of the sweat collector. As Figure 1a depicts, the inside of the chamber consists of five components: a double-sided adhesive, a thin layer of Technicloth, a microheater, a humidity and temperature sensor, and a lid. The double-sided adhesive attaches the Technicloth to the bottom of the chamber, covering the inlet. As such, when liquid passes through the collector's inlet, the Technicloth wicks the liquid into the chamber and uniformly distributes the liquid across the base of the chamber. The heater is then carefully positioned above the Technicloth, which expedites the evaporation of the liquid. The humidity and temperature sensor is then positioned at the top of the chamber which enables continuous readout of the chamber's climate. As seen in Figure 1b, the heater is positioned to not block the humidity and temperature sensor. Last, the lid closes the chamber and has two specially designed holes that permit the exit of evaporated water molecules as seen in Figure 1c. When both components are combined, the resulting device takes on a compact shape suitable to be worn on a forearm, as shown in Figure 1d,e.

2.2. Device Design

Across the human body, there are roughly two million functional sweat glands with some bodily locations containing many more than others.[34] The distribution of these glands is unbalanced, with some locations such as the fingers having 530 glands cm^{-2}, and others such as the chest containing 21 glands cm^{-2}.[34] When choosing a suitable body location to test the device on, the sweat gland densities and the comfortability of the location were the primary factors considered. Consequently, the ventral forearm was chosen as it has a large sweat gland density (159 glands cm^{-2}) and allows for the device to be easily worn during sedentary and exercise activities.[34] In addition, the sweat collector's performance on the forearm yielded consistent and reliable results during on-body trials in our previous work.[22]

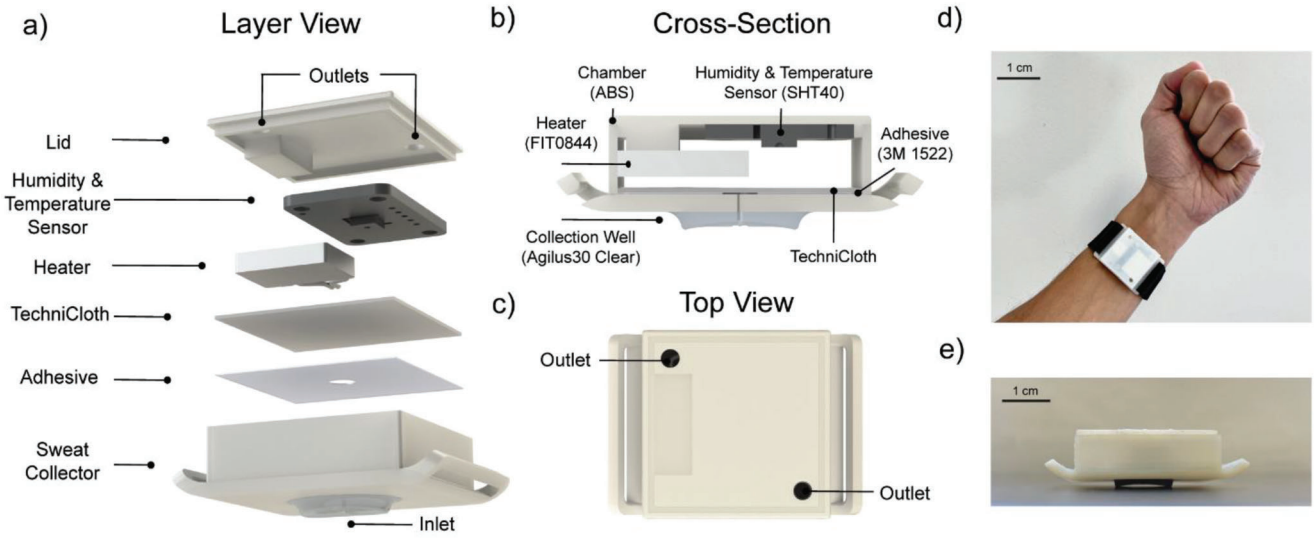

Figure 1. Wearable device to monitor sweat rate from the change in sweat-induced humidity levels. a) Layer-by-layer stack of the device structure and its components including a humidity and temperature sensor, a microheater, a Technicloth layer, double-sided adhesive, and the sweat collector. b) A cross-sectional schematic of the device when assembled and the materials used for each component. c) A top view of the device, showing the lid's two ventilation holes. d) The device worn on the ventral forearm. e) A cross-sectional view of the standalone device after assembly.

While the principle design components of the sweat collector from our prior work were used in this device, the sweat collector's curvature and area were tuned to ensure that the device's humidity chamber does not oversaturate during periods of exercise. In particular, since this device measures sweat-induced humidity levels, it was a critical design challenge to ensure that the flow of sweat into the chamber was controlled. A sweat collector with a large surface area may allow too much sweat to enter the chamber at once, which would fully saturate the air within the chamber and yield inconclusive humidity readings; on the other hand, a sweat collector with a small surface area may not allow enough sweat to enter the chamber at once, which would in turn insignificantly increase the chamber's humidity. With these considerations in mind, the sweat collector's surface area was set to 1.14 cm^2 with a curvature depth of 2 mm, which proved to be watertight and comfortable for this study's experiments, consistent with our prior publication's empirical testing of these qualities.[22]

Once sweat accumulates in the sweat collection well and moves through the inlet via the induced secretion pressure, it reaches the humidity chamber. The frame of the sweat collector and the humidity chamber are 3D-printed with a non-stretchable and sturdy digital acrylonitrile butadiene styrene (ABS). The chamber is 3 cm × 3 cm × 0.9 cm with two ventilation holes at the top with diameters of 0.25 cm. The chamber's objective is to evaporate the water molecules that enter and track the change in vapor pressure. In order to maximize the amount of volume evaporated over time, a thin slice of Technicloth covers the floor of the chamber. Consequently, when water enters the chamber, the water molecules are absorbed and spread across the floor uniformly, maximizing the surface area of liquid water within the chamber. Without the addition of a heater, the evaporation rate of the sweat would predominantly rely on the ambient temperature. At room temperature and low humidity, the evaporation rate of water within the chamber is slow and can quickly be outpaced by sweat rates during exercise periods. Thus, without intervention, the chamber would achieve maximum humidity levels quickly, which hinders the ability to analyze the change in humidity, and thus sweat rate. To remedy this, a microheater was introduced and placed with sufficient spacing from the Technicloth. With higher temperatures within the chamber, the evaporation rate increases. At the same time, the saturation vapor pressure increases, thus increasing the range of observable relative humidity levels. With sufficient ventilation, the device can capture a wide range of humidity levels, which is qualitatively displayed in **Figure 2**.

The placement of the microheater was determined to be off-centered and below the humidity and temperature sensor to avoid interference, which may cause a temperature gradient within the chamber, affecting the evaporation rate. To validate the effect of the microheater placement, a thermal simulation of the device was created using COMSOL (see Experimental Section). As shown in Figure S2, Supporting Information, when the device is worn on-body the heat distribution at the base is roughly uniform. Nonetheless, this effect is captured when calibrating the device and establishing a relative humidity baseline. In a future iteration of this device, a custom-shaped microheater and smaller humidity sensor could be used to achieve a more uniform temperature gradient within the chamber if desired.

The last design choice involved placing the humidity and temperature sensor on the lid of the chamber, which has two holes that permit the exit of water vapor. With this source of ventilation, the heater's effect becomes twofold as it also increases the temperature differential between the chamber and the environment, expediting the flow of water molecules out of the chamber. After performing preliminary controlled tests, the exact dimensions and spacings of the chamber components were finalized and put to the test in various off-body and on-body trials

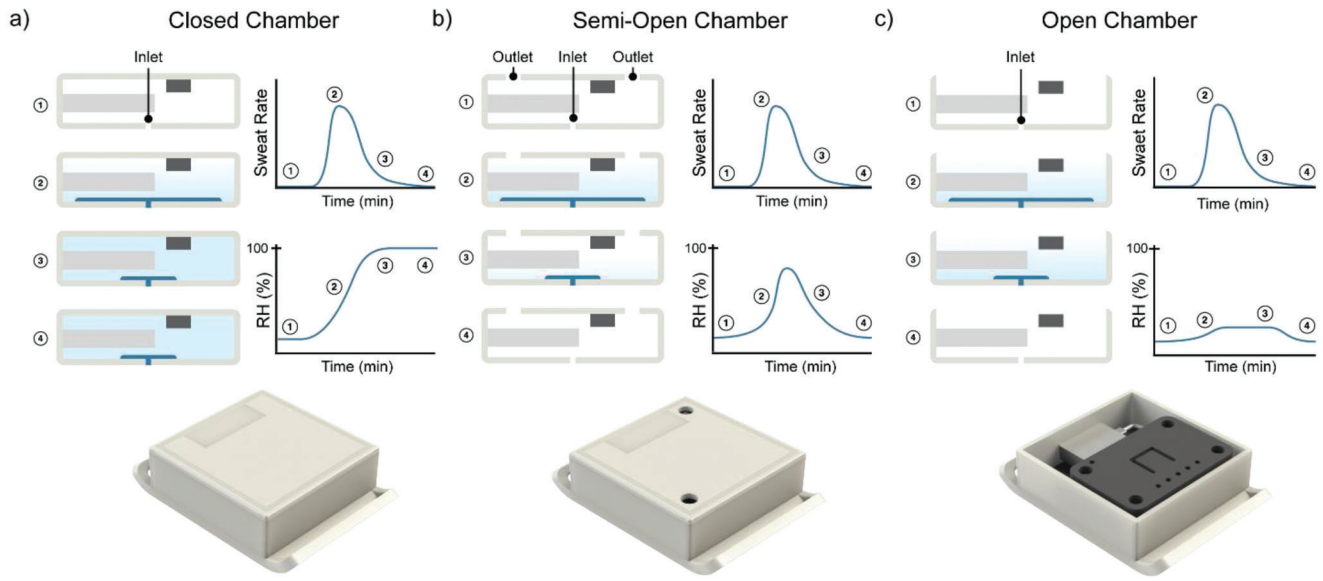

Figure 2. Illustration of the sweat rate and relative humidity curves exhibited when sweat enters our device at different ventilation levels: closed chamber, semi-open chamber, and open chamber. a) When sweat enters a closed chamber through the inlet, it evaporates quickly and saturates the chamber completely, flatlining the relative humidity curve at 100% since there is no outlet. Figure S1, Supporting Information, illustrates a trial where this phenomenon was exhibited. b) When sweat enters a semi-open chamber, like our device, through the inlet, the relative humidity increases significantly and then decreases back to the baseline as water vapor exits through the outlets. c) When sweat enters a completely open chamber through the inlet, the relative humidity curve increases insignificantly due to the quick movement of water vapor molecules into the ambient air.

2.3. Chamber Response Characterization

In order to understand the chamber's humidity and temperature dynamics, a benchmarking test was performed to determine the relationship between relative humidity and temperature within the chamber's confines. The experiment was conducted in an isolated and climate-controlled environment. As shown in **Figure 3**a, the chamber's relative humidity was measured at various microheater temperatures. The microheater's input voltage and current were supplied by a power supply unit. Each vertical dashed line in Figure 3a represents an increase in power supplied to the microheater. Four combinations of voltage and current values were tested (see Experimental Section), which yielded internal chamber temperatures of 22.3, 24.7, 26.5, and 30.0 °C, creating a mapping between the two. The time between vertical lines indicates the total time required for the chamber to reach the desired temperature and for a humidity baseline to be established. The dashed horizontal lines indicate the baseline humidity levels that each temperature level corresponded to within the chamber. As an example, the chamber took 40 min to reach 24.7 °C, which maintained a relative humidity of 45% (Figure 3a). By testing increasingly warmer temperatures within the chamber, valuable insight into the microheater's power consumption and sustainable temperature range was afforded. These results suggested that long-term (12–24 h) usage of the device in future, on-body experiments may require multiple commercial batteries in order to sustain in-chamber temperatures of up to 30.0 °C. The results also provided insight into which temperature values to target when performing tests with water or sweat. Importantly, there is a tradeoff between increasing chamber temperature and the resource and time practicality of such. On the one hand, as chamber temperature increases, humidity decreases, increasing the range of observable relative humidity levels should water be introduced into the system; on the other hand, increasing the chamber temperature comes at the cost of more power and longer ramp-up times. So, while a temperature higher than 30.0 °C may be more desirable because of its lowering effects on the chamber's humidity, the continuous power requirements, and time to reach that temperature may be impractical.

After compiling the results from Figure 3a, further analysis was performed to compare the relationship between humidity and temperature within the chamber to its theoretical relationship. In Figure 3b, the experimental and theoretical relationships are compared. The experimental data points are drawn from Figure 3a, where each point represents the temperature the heater was set to and the corresponding baseline humidity it achieved. The theoretical data points are calculated via Magnus's formula, which establishes a relationship between temperature and relative humidity when the ambient temperature, ambient humidity, and initial chamber humidity and temperature are known (see Experimental Section).[35] This phenomenon is illustrated in Figure 3c, where each stage in Figure 3a is depicted. As the chamber temperature increases, the air within the chamber can hold a greater number of water molecules, expanding the range of observable relative humidity levels. Given an ambient temperature of 22.3 °C and 50% relative humidity, the dew point was calculated to be 11.4 °C, which means that the relative humidity would be 100% at this temperature and that the air cannot hold any more water vapor, so additional water starts to condense. When the heater is powered, the temperature of the chamber increases which allows the air to hold more water molecules, so the relative humidity decreases. An even higher chamber temperature could be considered, however, power consumption and safety issues would arise.

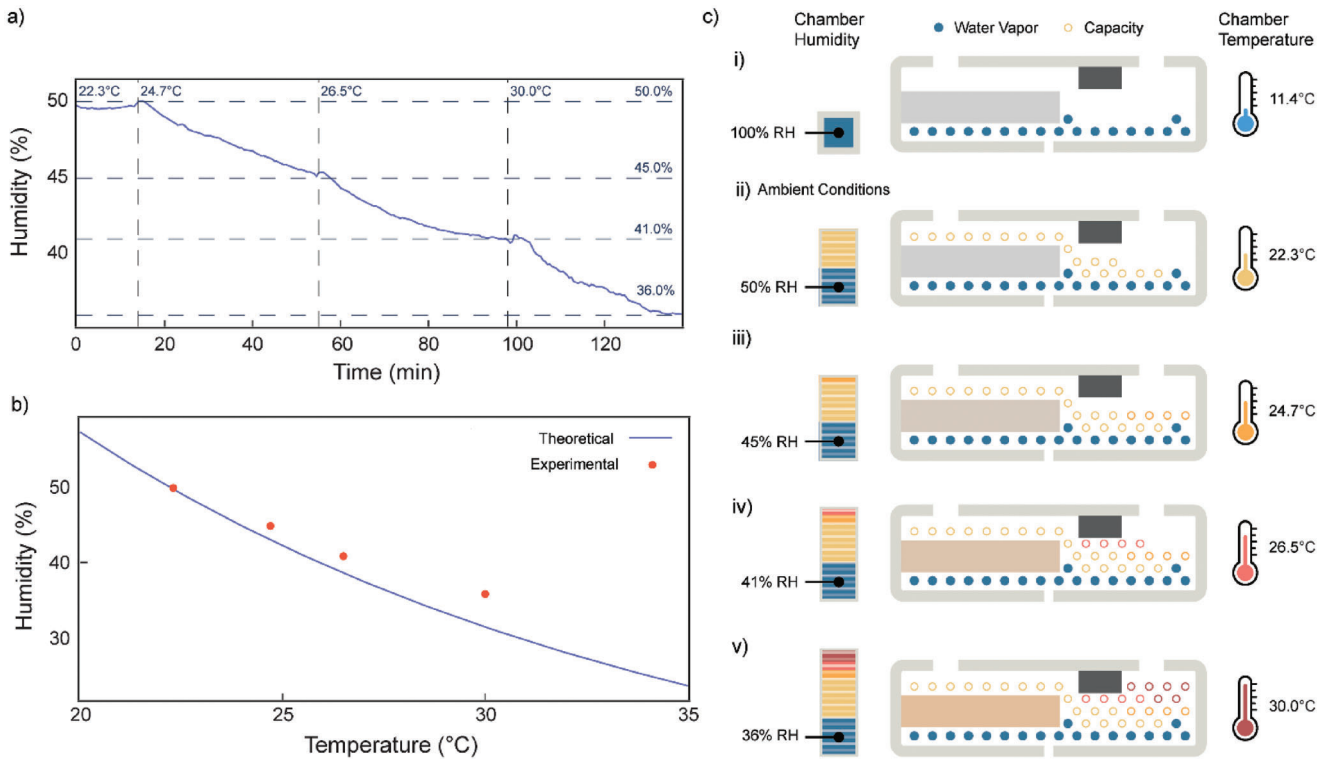

Figure 3. The chamber humidity response as a function of chamber temperature. a) The chamber humidity response when the microheater is set to different temperature levels. The vertical dashed lines indicate when the heater was set to the corresponding temperature after reaching a relative humidity baseline. b) The humidity versus temperature of the chamber. The blue line represents the theoretical curve computed via Magnus's equation and the red dots represent the empirically collected humidity versus temperature data points from (a). c) Graphic representation of the chamber temperature's dependence on relative humidity. Water vapor is represented as solid circles and blue rectangles on the chamber diagrams and the bar diagrams, respectively. Air capacity to hold more water vapor is represented by hollow circles and non-blue areas. i) Dew point calculated from ambient conditions. ii) Measured ambient conditions, when the microheater is turned off. iii–v) As the microheater is set to increasingly higher temperatures, the water molecule capacity increases, causing the relative humidity to drop.

Furthermore, Figure 3b suggests the empirical relationship between temperature and humidity is in line with the expected relationship, with an error of about 5%. We suspect part of this error is due to the 2% error that the off-the-shelf humidity sensor presents.[36] Importantly, however, the results indicate that our device's internal humidity correctly decreases as temperature increases and that our humidity readings are accurate within 5%. With this validation in hand, further experiments were ready to be conducted with water or sweat introduced into the system.

2.4. Performance under Controlled Conditions

In order to determine the device's response and resilience to the introduction of water into the system in a controlled setting, two experiments were performed by injecting various volumes of water into the chamber. For both off-body experiments, the device was first placed in an environment with minimal ambient temperature and humidity fluctuations and was positioned in a manner such that the sweat collector faced the ceiling—mimicking the orientation of the device if positioned on the ventral side of a forearm. Then, the device's microheater was powered by a power supply unit and was set to a fixed power level based on the findings from Figure 3a. Once the chamber temperature reached 30 °C and a baseline humidity level was established, the device was ready to receive water injections. For both experiments, this process took around 30 min. The baseline humidity levels for the two experiments differ due to the differences in ambient temperature and humidity between experiments. Moreover, **Figure 4**a illustrates the experiment setup and the process of injecting water. Once a fixed amount of water is injected into the system with a micropipette, the liquid evaporates and eventually flows out of the chamber via the ventilation holes in the lid. The continuous readout from the humidity and temperature sensor was then used to analyze this process.

In the first experiment, 2 µL of deionized water was injected into the chamber with a micropipette. Once the humidity response had been received and the chamber humidity returned to the baseline, this process was repeated two more times. Figure 4b illustrates the chamber humidity response after each injection, where the vertical dashed lines indicate when the water was injected. After each injection of 2 µL, the chamber's humidity level peaks within 2 min and eventually returns to the baseline after 30 to 35 min. For each injection, the difference between the peak humidity level and the baseline humidity level was almost within 1% of each other (16.4%, 17.0%, and 15.9%). In addition, the chamber temperature variation remained minimal. The results from this experiment demonstrate that the device produces

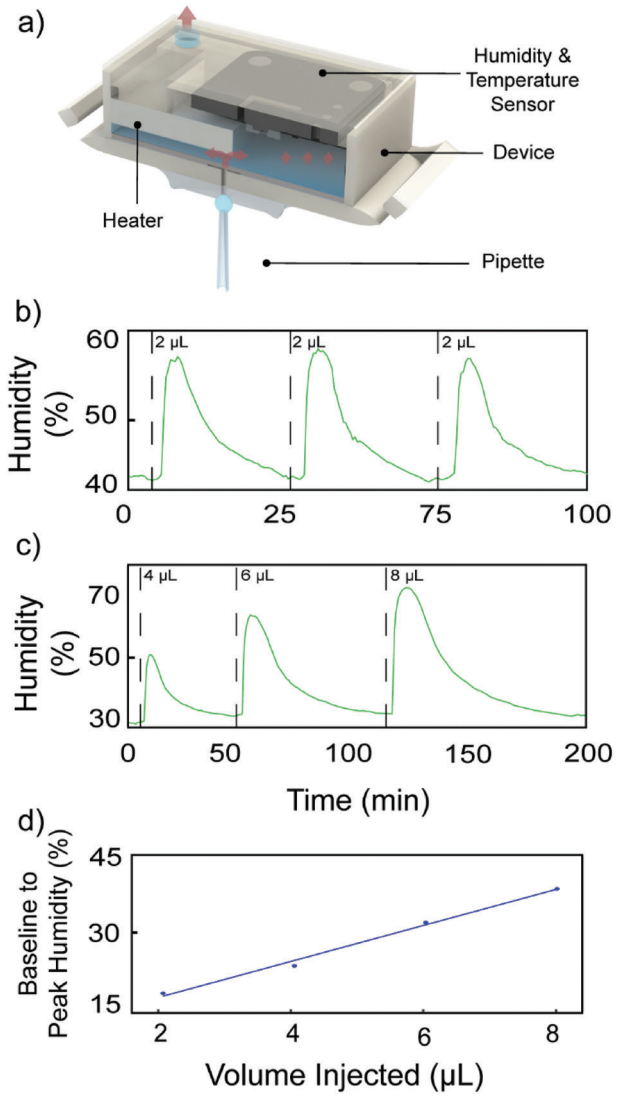

Figure 4. The chamber's humidity level over time when various volumes of deionized water are injected directly into the chamber. a) A schematic of the experiment setup where a micropipette is used to inject a fixed amount of liquid. Red arrows are also included to indicate the evaporation and exit of water molecules within the chamber. b) The humidity in the chamber versus time following a series of three independent injections of 2 µL of water. The vertical dashed lines represent when the water was injected. c) The humidity in the chamber versus time following a series of three independent injections of increasing volume: 4, 6, and 8 µL. The vertical dashed lines represent when the water was injected. d) The blue line represents the ordinary least squares line for the off-body dataset ($N = 4$) as presented: $y = 4.5x + 6.9$, $R^2 = 0.99$.

consistent and reproducible humidity curves when a fixed volume of liquid is injected in a climate-controlled environment.

In order to test the device's ability to handle larger volumes of liquid, a second experiment was conducted where the volume of liquid injected into the chamber increased after each injection. In this experiment, 4, 6, and 8 µL of deionized water were injected and their corresponding humidity responses were recorded. Figure 4c illustrates the results from the experiment and the varying humidity curves. For each of the three volumes tested, their respective changes in chamber humidity were 22.8%, 34.1%, and 42.5%. In addition, the time it took for each instance to return to the baseline humidity also increased with each progressive volume, ranging from 40 to 70 min. The results from this experiment indicate that as the input volume increases, the change in the chamber's humidity level increases. Importantly, the changes in humidity for the four volumes (2, 4, 6, and 8 µL) tested in these experiments are noticeably different, which ultimately prompted analysis to determine their relationship.

In order to analyze the relationship between the amount of water injected and the change in humidity within the chamber, the baseline-to-peak humidity difference was computed for each curve. More specifically, the baseline humidity level was subtracted from the peak humidity level for each injection. While more data points would be needed to make more precise conclusions, the relationship between the baseline-to-peak humidity and the volume of water injected appears linear between 2 and 8 µL given the strong coefficient of determination ($R^2 = 0.99$, Figure 4d). While these experiments provide valuable insight into the reliability and reusability of the device with effectively fixed sweat rates, experiments that gauge the device's response to variable sweat rates must be conducted.

2.5. Performance when Worn during Exercise

The subsequent experiment tested the device's performance when worn by a subject exercising. To further understand the relationship between the sweat-induced humidity and the amount of sweat secreted, the subject was asked to exercise while wearing a heart rate monitor, our humidity-based sweat rate sensor, and a microfluidic-based sweat rate sensor. **Figure 5**a is a photograph taken of the subject with these three sensors worn on the ventral side of their forearm. Once the humidity and microfluidic sensors were connected to their respective power supplies and boards, the subject was instructed to walk on a treadmill at a comfortable pace of 3 mph. Once the humidity device reached a stable temperature of 35 °C and a humidity baseline had been reached, the subject began walking. It is important to note that the device's internal temperature was a few degrees warmer than that of the prior off-body experiments because the device is attached to the subject's body, which is an added source of heat. Thus, controlling the exact temperature level within the chamber was much more difficult. During the trial, the humidity sensor transmitted chamber humidity data every 30 s to a smartphone, and the subject's sweat loss volume was recorded every 2 min by observing the microfluidic device's fill level. Figure 5b compares the subject's walking speed, heart rate, total sweat loss, and sweat humidity during the 80 min trial. The bottom two panels display an observable relationship between the total sweat lost and the sweat humidity within the chamber. Figure 5b indicates that the humidity levels began to increase before sweat was collected in the microfluidic device. In addition, when the subject stopped walking at 60 min, the total sweat lost began to plateau and the humidity within the chamber started its descent. Thus, the humidity sensor when worn can detect the onset of sweat quicker than the microfluidic device and presents promising sensitivity to a subject's exercise trends.

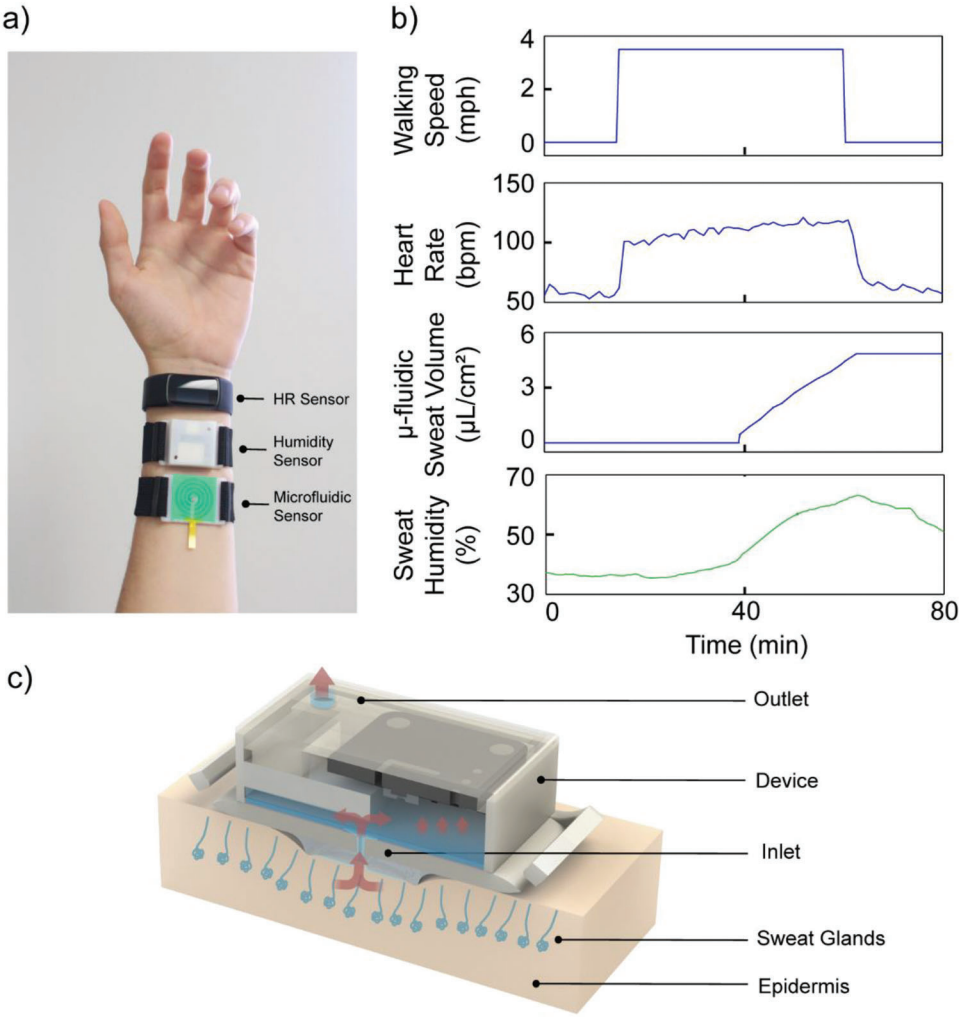

Figure 5. On-body experiment setup and results from an 80 min, exercise trial. a) During the trial, the subject wore a Fitbit to monitor heart rate, our humidity-based sweat rate sensor, and a microfluidic-based sweat rate sensor. b) The subject's walking speed, heart rate, total sweat loss, and sweat humidity throughout the entire trial. c) A cross-sectional view of the device's interaction with the skin and arrows indicating the three rates involved in the system: sweat rate, evaporation rate, and the rate at which the water molecules exit through the ventilation holes.

To better understand the dynamics of the device when worn, it is important to analyze the forces involved in the system and the device's interaction with the skin's surface. In Figure 5c, the device's connection with the skin's surface is shown. Due to the sweat collector's curvilinear design, the device forms a tight and secure seal with the epidermis. A tight seal is necessary to ensure that leakage does not occur, which would prevent sweat's natural secretion pressure from propelling the sweat into the inlet. As sweat is secreted from the skin's surface, the liquid is piped into the chamber and subsequently spread evenly at the base of the chamber. In contrast to the off-body experiments, sweat is gradually secreted from the epidermis and thus, the chamber takes longer to reach a peak humidity. Once the liquid is in the chamber, there are two rates to consider: the evaporation rate of the liquid and the rate at which water vapor molecules exit the chamber through the lid. The inclusion of the microheater affords some control over these rates.

2.6. Performance when Worn for Long Periods of Time

Next, we tested the device's performance when worn throughout a day. The objective of this experiment was to evaluate the performance of the device over a long period of time, specifically 12 to 16 h, and to analyze its sensitivity to sedentary and physical activities. The device was placed on the ventral forearm of a healthy subject along with a heart rate sensor and a microfluidic-based sweat rate sensor. The heart rate sensor was used to monitor the subject's heart rate, while the microfluidic-based sensor was used to monitor the sweat rate of our subject. The setup was nearly identical to that of Figure 5a, however, a small 3D-printed housing for a 5V battery was also attached to the subject's forearm. This way, the device could be powered throughout the day and if the battery ran out of charge, a replacement battery could be swapped in. The device was continuously worn for a 15 h period. The subject was asked to perform their typical daily activities, including sleeping, eating, and driving, with the addition of

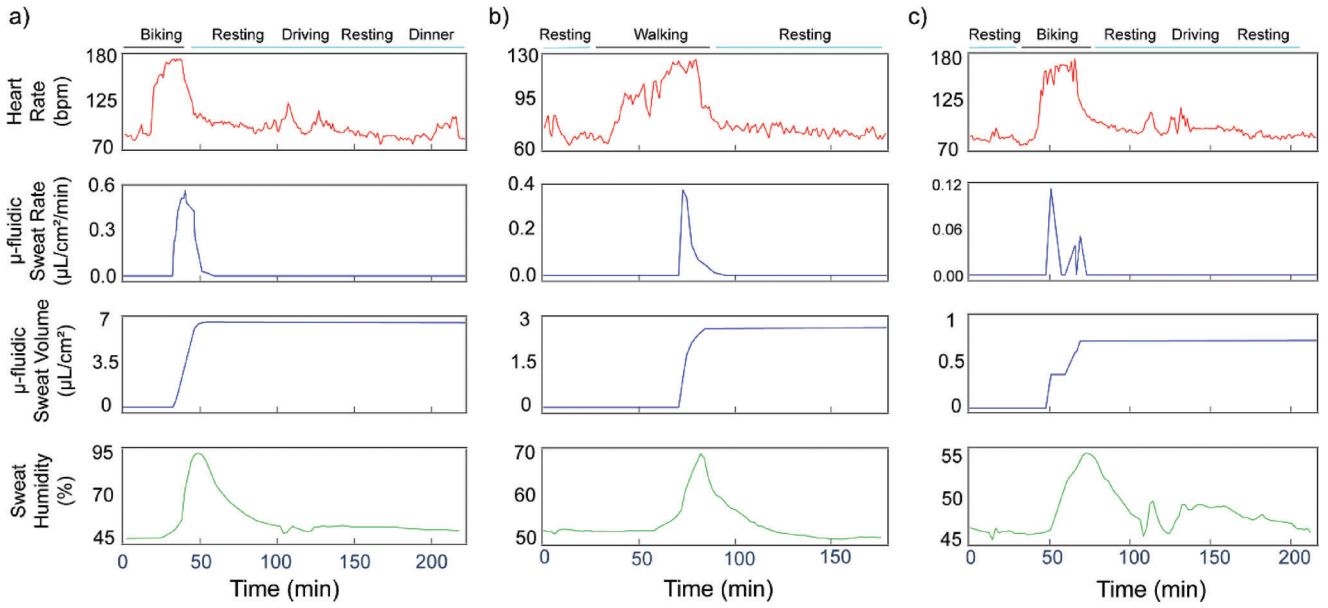

Figure 6. The results from a 15 h, on-body experiment where the subject was asked to perform normal daily activities in addition to three segments of physical activity. Each panel is a 3–4 h section of the 15 h trial when the subject was instructed to walk or bike. The subject's heart rate, sweat rate, total sweat loss, and sweat-induced humidity levels are shown. The time between each section was spent replacing the battery of the device and recalibrating the chamber temperature and humidity baselines. a) The subject biked at an intense speed of 15 mph for 20 min and proceeded to rest, drive, and eat. b) The subject walked at 3 mph for 40 min and proceeded to rest. c) The subject biked at a mild speed of 5 mph for 25 min and proceeded to rest and drive.

physical activities like walking and biking. Three segments during this period are displayed in **Figure 6**. Each segment represents a 3–4 h period during the trial where the subject either biked or walked. In the time between these segments, the battery of the device was replaced to ensure the microheater had sufficient power to maintain chamber temperatures of 35 °C. Each panel in Figure 6 illustrates the heart rate, microfluidic sweat rate and sweat volume, and the sweat-induced humidity levels during each activity. During the physical activities of walking and biking, the sweat humidity and sweat rate increased in tandem for each period, indicating that the device is sensitive enough to physical activities and can be worn for long periods of time.

2.7. On-Body and Off-Body Statistical Comparison

After performing these short-term and long-term experiments, the next objective was to perform more on-body experiments and to capture the relationship between humidity and sweat volume. Four different subjects were then asked to participate in an exercise trial where they would either bike or walk for 60 min. In a similar fashion to the methodology behind the Figure 5 experiment, the heart rate, humidity, and microfluidic sensors were placed on the subject. Once the relative humidity inside the chamber reached a baseline, the subject began to exercise. After each trial, the humidity and sweat loss curves were compiled and analyzed. Similarly to the computation performed for Figure 4d, the difference between the baseline and peak humidity was compared to the total amount of sweat secreted. In addition to these added four trials, this computation was performed on each instance of exercise in Figure 6, giving a total of seven data points.

Together, these seven on-body data points and the line of best fit were plotted in **Figure 7**, along with the four off-body data points presented in Figure 4d for comparison. Between 2 and 8 μL, the relationship between the on-body baseline-to-peak humidity difference and the volume of sweat secreted appears linear given the coefficient of determination ($R^2 = 0.83$, Figure 7). The relationship between the off-body baseline-to-peak humidity difference and the volume of liquid injected also appears to be linear between 2 and 8 μL ($R^2 = 0.99$, Figure 7). As the amount of liquid entering the device increases, the baseline-to-peak humidity tends to increase at similar rates for both the on-body

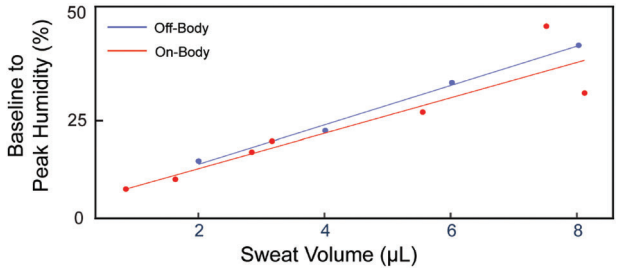

Figure 7. The relationship between the baseline-to-peak humidity levels and the volume of liquid injected or secreted for both the on-body and off-body datasets. The red line represents the ordinary least squares line for the on-body dataset ($N = 7$): $y = 4.1x + 6.9$, $R^2 = 0.83$. The blue line represents the ordinary least squares line for the off-body dataset ($N = 4$) as presented in Figure 4d: $y = 4.5x + 6.9$, $R^2 = 0.99$.

and off-body settings (4.1% μL^{-1} and 4.5% μL^{-1}). The intercepts for the on-body and off-body settings are equal (6.9%). Thus, as the volume of liquid entering the system increases, the on-body model predicts an increasingly lower baseline-to-peak humidity than that of the off-body model.

Despite the similarities between the on-body and off-body models, it is important to recognize that the on-body model has a relatively low R^2, which indicates that a linear fit does not account for all of the variability in the data. This is presumably due to the small sample size ($N = 7$) and the added variability factors during the on-body experiments such as varying ambient temperature, ambient humidity, and the subject's sweat profile and sweat rate. On the other hand, the large R^2 value for the off-body model indicates that a linear fit is ideal, however, the small sample size ($N = 4$) prevents any definitive conclusions about the variance of the model. Nonetheless, the two models are aligned and give valuable insight into the baseline-to-peak humidity and volume of sweat relationship between 2 and 8 µL. In the future, more on-body trials will be conducted to further solidify the relationship.

In addition, it is worth mentioning that there were small temperature fluctuations inside the chamber during our on-body experiments. These fluctuations could be caused by a number of reasons, such as electrical current instability from our power supply, the introduction of water into the chamber, changes in body temperature, or changes in ambient climate. While the combination of these external factors is difficult to assess numerically, we computed an estimate of the error in the peak humidity reading as a result of chamber temperature fluctuations. As shown in Figure S3, Supporting Information, the maximum chamber temperature fluctuation during on-body experiments was 2 °C. These fluctuations in chamber temperature yielded a maximum humidity reading error of 4% at the peak, using the Magnus equation to adjust for temperature variations between the start of the experiment and when the peak humidity was recorded. In order to reduce our margin of error, we could convert our measurements to absolute humidity, which accounts for temperature variability. As seen in Figure S4, Supporting Information, the absolute humidity is plotted against time and compared to relative humidity. Since the absolute humidity curve follows the same trend as the relative humidity curve, and our analysis is based on baseline-to-peak humidity, which is a relative value, we decided to keep relative humidity in our analysis to avoid adding complexity.

While the models present similar lines of best fit, it must also be recognized that the method of sweat entry into the chamber for the on-body and off-body experiments was different. During the on-body experiments, sweat entered the chamber at a rate proportional to the subject's forearm sweat rate. From the microfluidic-based sensor results, these rates are on the order of 100 nL min^{-1}. However, during the off-body experiments, sweat was injected directly into the chamber within 1 min. So, the effective sweat rates in the off-body experiments were on the order of 1000 nL min^{-1}. As a result, the time it takes for the chamber to reach a peak humidity level in the off-body trials is much shorter than in the on-body trials. We believe the differences in the rate of liquid entry between both experiments are explained by the differing slopes between the on-body and off-body models. Since it takes longer for the total volume of sweat to enter the device's chamber in the on-body trials, a small amount of water vapor exits the chamber via the ventilation holes. Thus, the peak humidity level would be a slight underestimate of the expected humidity level, which is seen in Figure 7.

Moreover, the device's ability to perform similarly in both on and off-body settings affords greater insight into the relationship between sweat-induced humidity levels and the total volume a subject sweat. While more trials with this device would need to be conducted to make more affirmative claims about the numeric relationship between the two, the results from these experiments present a promising approach to calculating continuous sweat rates from baseline-to-peak humidity levels.

3. Conclusion

Our wearable device monitors a user's sweat expenditure during sedentary and physical activity by measuring their secreted sweat humidity levels and can be worn for long periods of time without oversaturating or overfilling. The device's semi-open chamber, consisting of a microheater and humidity sensor, continuously monitors the humidity of a user's skin sweat. The objective is to compare the change in humidity versus the volume of sweat secreted. After testing the device in both off-body and on-body settings with varying climatic conditions, we determined that there is a promising relationship between the amount of sweat an individual secretes and the change in the corresponding humidity curve. While a concrete formulation to relate the two will require more on-body trials to be conducted, the initial findings are promising and lend this device to usage alongside a microfluidic-based device. In addition, given the device's reliance on measuring precise humidity levels within the semi-open chamber, we envision further work to analyze the device's performance in extremely humid or cold climates. As the device was designed with off-the-shelf components, we believe future iterations of this device can be made with microscale components which will improve the device's power consumption and wearability. In addition, we believe that this device's form factor may lend itself to future versions that track volatile organic compounds or trace alcohol contents in a user's sweat. With that being said, we believe this device can potentially be used to continuously monitor exercise sweat rates either stand-alone or in conjunction with other microfluidic-based devices.

4. Experimental Section

Device Fabrication: A humidity and temperature sensor (SHT40) and a microheater (FIT0844) were purchased from DigiKey Electronics. TechniCloth Nonwoven Wipers (55% cellulose and 45% polyester) were purchased from Texwipe. Double-sided medical tape (1522) was purchased from 3M. Objet Polyjet Model Materials: digital ABS (RGD531, RGD515) and Agilus30 Clear (FLX935), a rubber-like photopolymer, were provided by the Jacobs Institute for Design Innovation. An elastic band (Dreamlover elastic sewing band 2.5cm × 11m) was purchased from Amazon. Figure 1b provides a visual diagram of the aforementioned materials and components.

The device consists of two main components: the collection well and the chamber. A detailed description of the fabrication process of the collection well was included in a previous study.[22] In brief, the two components were 3D-printed together. The collection well was 3D-printed in Agilus30 Clear, a PolyJet photopolymer that was tear-resistant and flexible. The chamber was 3D-printed with a 2:1 mixture of RGD531 and RGD515,

two hard digital ABS materials. An Objet260 3D printer was used to print the curvilinear collection well on top of a soft support structure (FullCure SUP706). The scaffolding was then removed via the use of a water jet and finally cleaned with isopropyl alcohol. After curing, the inlet hole connecting the chamber and the collection well was cleaned with a 1 mm diameter needle and isopropyl alcohol. When the device was used for on-body experiments, an elastic band was threaded through the device.

The internal components of the chamber were then placed carefully. The double-sided adhesive was secured to the base of the chamber, followed by a piece of Technicloth. The adhesive has a circular cutout in the middle that aligns with the inlet, such that incoming sweat was absorbed into the Technicloth. Then, the humidity and temperature sensor was fixed to the lid of the chamber, along with the microheater.

Device Parameter Optimization: The core parameters related to the chamber humidity detection were chamber temperature, outlet hole size, heater positioning, sweat collection area, and the distance between the heater and the evaporation plane. Preliminary iterations of the device specifically focused on tuning chamber temperature, the number of outlet holes, and the size of each outlet hole.

Heating power was varied at different levels in Figure 3 to determine the range of possible chamber temperatures and the time it takes the off-the-shelf resistive heater to reach each temperature level. The device requires the chamber temperature to be slightly above the ambient temperature to improve evaporation rates and establish a baseline relative humidity.

The heating area, or the chamber's base area, was set to match the area of the collection well. It was found that the dimensions of this base area and the subsequent Technicloth layer were large enough to ensure that a thin layer of sweat could persist even at high exercise rates. If the collection well area was increased beyond 1.14 cm,[2] a larger base area would be expected to be needed to ensure that sweat was uniformly distributed across the base. In this case, after conducting the in vitro experiments with 8 µL, corresponding to a high sweat rate, the outer perimeter of the Technicloth was not saturated. Further optimization of this component was analyzed and discussed in the prior paper.[22]

The microheater positioning was determined to be off-centered and below the humidity and temperature sensor to avoid interference. As shown in Figure S2, Supporting Information, a thermal simulation of the device when worn on-body was created using COMSOL to validate this configuration. A stationary heat transfer in solids study was computed using a simplified version of this model. The boundary conditions were set to 25 °C for air, 34 °C for the microheater, and 34 °C for skin temperature at the forearm. As expected, a gradient was seen toward the top of the device in Figure S2a, Supporting Information, due to the outlets. As shown in Figure S2b, Supporting Information, on the other hand, the heat distribution was slightly off-centered but radial at the base of the chamber, roughly following the pattern of sweat distribution along the Technicloth when introduced into the device. While a uniform heat distribution across the entire base was optimal, the current heat distribution ensured that most of the sweat was evaporated at the same temperature. However, this effect was captured when calibrating the device and establishing a relative humidity baseline. In a future iteration of this device, a custom-shaped microheater could be used to achieve a more uniform temperature gradient within the chamber if desired.

The distance between the heater and the evaporation plane was set to 0.19 cm. From an assembly standpoint, this spacing was practical. In principle, this spacing could be reduced in conjunction with minimizing the volume of the chamber. In future iterations, miniaturizing this device which would significantly improve power usage and evaporation speeds was envisioned.

Microfluidic Sweat Rate Sensor Device Fabrication: The microfluidic sweat rate device, used to measure sweat rate and total sweat loss during exercise periods, was extensively tested and detailed in a prior study.[22] In brief, the device consisted of two main components: the sweat collector and the microfluidic layers. The sweat collector used in this device was identical to the one used for the device presented in this paper. The microfluidic layers consisted of a laser-cut microfluidic channel sandwiched between a capping layer and an electrode layer. The electrode layer was roll-to-roll printed and consisted of embedded electrodes. When sweat enters the microfluidic and more electrodes come in contact with the sweat, a stronger signal was emitted, and the exact amount of sweat collected can be calculated via a smartphone application. Prior to each on-body experiment, a new microfluidic-based sweat rate sensor was fabricated.

Chamber Characterization: The chamber, measuring 3.0 cm × 3.0 cm × 0.9 cm, was 3D printed on top of the sweat collector. A rectangular hole (1.75 cm × 0.25 cm) was made on one side of the chamber to allow the wires connecting the microheater to a power supply and the humidity and temperature sensor to a microcontroller (ESP32). The lid of the chamber also consists of two holes with diameters of 0.25 cm. These two lid holes, along with the wiring hole, were essential to the ventilation of the chamber. The same device was used for all the on-body and off-body trials. Between trials, the device's collection well was thoroughly cleaned with isopropyl alcohol.

The calculation of the chamber's humidity-to-temperature relationship was performed using the Magnus formula for temperatures between −45 and 60 °C.[35] Given the ambient temperature and humidity, and an initial condition for the humidity and temperature within the chamber, this equation relates the saturation vapor pressure and the dew point of the chamber. With these values, the expected humidity for a given temperature can be determined. In this case, the trial in Figure 3a was performed at an ambient temperature of 22.3 °C and ambient humidity of 50.0%.

Electrical Components Characterization: The microheater (FIT0844) used to heat the chamber during the experiments was a thermistor that can reach 40 °C and had a maximum power intake of 3W. For off-body experiments, the microheater was continuously powered by a power supply unit with 450 mW. Four combinations of voltage and current values were used to achieve the different temperatures used in the benchmarking tests in Figure 3a: (0V, 0mA), (1.7V, 60mA), (2.5V, 80mA), (4.5V, 100mA) for 22.3, 24.7, 26.5, and 30.0 °C respectively. For on-body experiments, a commercial 5V battery and a voltage regulator were used to power the microheater. Prior to each trial, the heater was powered for 30 to 40 min to reach the desired chamber temperature.

The humidity and temperature sensor (SHT40) was used to continuously measure the chamber's internal climate. The sensor was listed to have a 1.8% relative humidity margin of error and a 0.2 °C margin of error.[36] The sensor was connected to an ESP32 microcontroller that supplied 5V. Custom Arduino code was written to send humidity and temperature values over BLE every 30 s. During each trial, the circuit was powered and an Android smartphone was used to continuously receive the humidity and temperature values. All the data were then concatenated and analyzed in a Jupyter Notebook.[37]

Off-Body Experiments: The off-body experiments were performed in well-regulated temperature and humidity conditions. The ambient temperature hovered between 22 and 24 °C while the ambient humidity ranged from 45% to 60%. The difference in baseline humidity levels within the chamber in Figure 4b,c was precisely due to differences in ambient humidity levels on the days of those experiments.

When it was ready to inject water into the system, a micropipette was used to measure and dispense the deionized water directly on top of the sweat collector's inlet. As the device was inverted during these tests, gravity would push the liquid through the inlet and into the chamber. As Figure 3b,c corroborate, this process created a short lag time of 1 to 3 min until the water began to enter the chamber. The Technicloth at the base of the chamber helped expedite this process by wicking the water molecules into the chamber.

Following each experiment, the humidity curve from this device was plotted against the amount of deionized water injected, and an ordinary least squares line was fitted.

On-Body Trials: All of the on-body trials with the exception of the 15 h trial were performed in a room with a less regulated environment in order to simulate device usage outdoors. The ambient temperatures during these trials ranged from 22 to 31 °C, while the ambient humidity levels ranged from 40% to 61%. As controlling the exact ambient temperature level was difficult when conducting the on-body trials, it was ensured

that the chamber temperatures prior to each experiment were equal to or greater than the ambient temperature. This decision validated that evaporation within the chamber was a result of the chamber's temperature. The ambient climate was continuously recorded via a secondary SHT40 humidity and temperature sensor that was placed in the room. The subjects chose to either walk on a treadmill or bike on a stationary bicycle (Gold's Gym Cycle Trainer 290C). In addition to the humidity-based sweat rate sensor and the microfluidic-based sweat rate sensor, the subjects wore a Fitbit fitness tracker (Fitbit Charge 3) to track heart rate.

Following each experiment, the humidity curve from this device was plotted against the sweat loss curve from the microfluidic device. The baseline-to-peak humidity difference was then computed. Then, for each trial, the peak of the sweat loss curve was used to estimate the true amount of sweat secreted during the exercise period. The amount of sweat secreted was plotted against the corresponding baseline-to-peak humidity and an ordinary least squares line was fit.

Each of the on-body experiments was performed using the same device and did not suffer from any structural integrity issues. The materials used to fabricate the device proved to be sturdy and durable, which was more extensively tested in the prior work that conceived the sweat collector.[22]

Supporting Information

Supporting Information is available from the Wiley Online Library or from the author.

Acknowledgements

This work was partially supported by the National Science Foundation through grant NASCENT-1160494, and by the Berkeley Sensors and Actuators Center (BSAC) and the Bakar Fellowship. On-body human trials were carried out at the University of California, Berkeley in compliance with the human research protocol (CPHS 2014-08-6636) approved by the Berkeley Institutional Review Board (IRB). Informed consent was obtained from the subjects before enrollment in the study.

Conflict of Interest

The authors declare no conflict of interest.

Author Contributions

A.A. and M.D. contributed equally to this work. A.A., M.D., and A.J. conceived the idea. A.A. and M.D. designed the experiments and performed the studies with the help of L.F.A.-C. A.A. wrote the manuscript with the help of M.D. and L.F.A.-C.A.A. and L.F.A.-C. designed the devices. A.A. and A.J. performed and interpreted the statistical analysis. L.F.A.-C. and A.W. performed thermal simulations. All authors discussed the results and revised the manuscript.

Data Availability Statement

The data that support the findings of this study are available from the corresponding author upon reasonable request.

Keywords

exercises, humidity, sweat rate, sweat rate sensors, wearable devices, hygrometer

Received: March 10, 2023
Revised: May 12, 2023
Published online:

[1] S. Xu, A. Jayaraman, J. A. Rogers, *Nature* **2019**, *571*, 319.
[2] T. R. Ray, J. Choi, A. J. Bandodkar, S. Krishnan, P. Gutruf, L. Tian, R. Ghaffari, J. A. Rogers, *Chem. Rev.* **2019**, *119*, 5461.
[3] H. U. Chung, B. H. Kim, J. Y. Lee, J. Lee, Z. Xie, E. M. Ibler, J. A. Rogers, *Science* **2019**, *363*, eaau0780.
[4] J. Dunn, R. Runge, M. Snyder, *Pers. Med.* **2018**, *15*, 429.
[5] W. C. Kuo, T. C. Wu, J. S. Wang, *Micromachines* **2022**, *13*, 1742.
[6] Z. Sonner, E. Wilder, J. Heikenfeld, G. Kasting, F. Beyette, D. Swaile, R. Naik, *Biomicrofluidics.* **2015**, *9*, 031301.
[7] L. C. Tai, T. S. Liaw, Y. Lin, H. Y. Nyein, M. Bariya, W. Ji, A. Javey, *Nano Lett.* **2019**, *19*, 6346.
[8] J. M. Moon, H. Teymourian, E. De la Paz, J. R. Sempionatto, K. Mahato, T. Sonsa-ard, J. Wang, *Angew. Chem., Int. Ed.* **2021**, *60*, 19074.
[9] J. Xiao, C. Fan, T. Xu, L. Su, X. Zhang, *Sens. Actuators, B.* **2022**, *359*, 131586.
[10] J. Moyer, D. Wilson, I. Finkelshtein, B. Wong, R. Potts, *Diabetes Technol. Ther.* **2012**, *14*, 398.
[11] J. R. Sempionatto, J. M. Moon, J. Wang, *ACS Sens.* **2021**, *6*, 1875.
[12] K. G. Foster, E. N. Hey, B. O'Connell, *Arch. Dis. Child.* **1971**, *46*, 444.
[13] L. B. Baker, *Temperature* **2019**, *6*, 211.
[14] M. J. Patterson, S. D. Galloway, M. A. Nimmo, *Exp Physiol.* **2000**, *85*, 869.
[15] J. Doolittle, P. Walker, T. Mills, J. Thurston, *Arch. Dermatol. Res.* **2016**, *308*, 743.
[16] L. B. Baker, C. T. Ungaro, B. C. Sopeña, R. P. Nuccio, A. J. Reimel, J. M. Carter, K. A. Barnes, *J. Appl. Physiol.* **2018**, *124*, 1304.
[17] W. C. Randall, C. N. Peiss, *J. Invest. Dermatol.* **1957**, *28*, 435.
[18] R. A. Oppliger, C. Bartok, *Sports Med.* **2002**, *32*, 959.
[19] J. T. Korpelainen, K. A. Sotaniemi, V. V. Myllylä, *Stroke* **1992**, *23*, 1271.
[20] W. P. Cheshire, R. Freeman, in *Seminars in Neurology*, Thieme Medical Publishers, New York **2003**, pp. 399–406.
[21] A. I. Vinik, M. Nevoret, C. Casellini, H. Parson, *Curr. Diabetes Rep.* **2013**, *13*, 517.
[22] M. Dautta, L. F. Ayala-Cardona, N. Davis, A. Aggarwal, J. Park, S. Wang, A. Javey, *Adv. Mater. Technol.* **2023**, *8*, 2201187.
[23] A. Koh, D. Kang, Y. Xue, S. Lee, R. M. Pielak, J. Kim, J. A. Rogers, *Sci. Transl. Med.* **2016**, *8*, 366ra165.
[24] H. Y. Y. Nyein, M. Bariya, B. Tran, C. H. Ahn, B. J. Brown, W. Ji, A. Javey, *Nat. Commun.* **2021**, *12*, 1823.
[25] Z. Zhang, M. Azizi, M. Lee, P. Davidowsky, P. Lawrence, A. Abbaspourrad, *Lab Chip.* **2019**, *19*, 3448.
[26] V. Jain, M. Ochoa, H. Jiang, R. Rahimi, B. Ziaie, *Microsyst. Nanoeng.* **2019**, *5*, 29.
[27] Z. Yuan, L. Hou, M. Bariya, H. Y. Y. Nyein, L. C. Tai, W. Ji, A. Javey, *Lab Chip.* **2019**, *19*, 3179.
[28] S. Wang, M. Liu, X. Yang, Q. Lu, Z. Xiong, L. Li, T. Zhang, *Biosens. Bioelectron.* **2022**, *210*, 114351.
[29] L. B. Baker, J. B. Model, K. A. Barnes, M. L. Anderson, S. P. Lee, K. A. Lee, R. Ghaffari, *Sci. Adv.* **2020**, *6*, eabe3929.
[30] M. Bariya, N. Davis, L. Gillan, E. Jansson, A. Kokkonen, C. McCaffrey, A. Javey, *ACS Sens.* **2022**, *7*, 1156.
[31] K. Kwon, J. U. Kim, Y. Deng, S. R. Krishnan, J. Choi, H. Jang, J. A. Rogers, *Nat. Electron.* **2021**, *4*, 302.
[32] J. Francis, I. Stamper, J. Heikenfeld, E. F. Gomez, *Lab Chip.* **2019**, *19*, 178.
[33] P. Salvo, F. Di Francesco, D. Costanzo, C. Ferrari, M. G. Trivella, D. De Rossi, *IEEE Sens. J.* **2010**, *10*, 1557.

[34] N. A. Taylor, C. A. Machado-Moreira, *Extreme Physiol. Med.* **2013**, *2*, 4.
[35] SHTxx Humidity & Temperature – Dew Point Calculation, http://irtfweb.ifa.hawaii.edu/~tcs3/tcs3/Misc/Dewpoint_Calculation_Humidity_Sensor_E.pdf (accessed: February 2023).
[36] SHT3x–SHT4x Transition Guide, https://sensirion.com/media/documents/9B40ED17/638A0562/Sensirion_Transition_Guide_SHT3x-SHT4x.pdf (accessed: February 2023).
[37] A. Aggarwal, Wearble Humidity Sensor Algorithms and Computation, https://github.com/aaggarw99/Humidity-Based-Sensor-Algorithms (accessed: October 2022).